Modeling of Jellyfish-inspired Robot Enabled by Dielectric Elastomer

Shengbin Wang · Zheng Chen*

Received: date / Accepted: date

Abstract Bio-mimetic robots can provide better camouflage effect to explore the seabed by mimicking the swimming locomotion of aquatic creatures. Jellyfish-like robot is a type of unmanned underwater robot can help us explore marine ecosystems and complex underwater ecology efficiently since they can swim steadily with its symmetrical structure that has been optimized in nature and generate sufficient jet propulsion with low power input. The developed jellyfish robot in this paper exhibits contracting muscle-like behaviour. It combines a dielectric elastomer (DE) diaphragm actuator with a transmission mechanism, which can provide compliant thrust force to propel the jellyfish robot to transit through water. This paper presents the design, fabrication, modeling, and experimental characterization of the novel jellyfish robot. A sawtooth signal with specific amplitude and frequency is chosen as input signal that leads to expansion and shrinking of the jellyfish bell. The simulation results from the observed two steps in a cycle of movement are quantitatively similar with the experimental outputs. A data-driven model is developed to capture the vibration in the first step. The process of contracting the bell and producing thrust force is captured by a physical model in the second step. The preliminary results show the jellyfish robot can swim underwater effectively in the vertical direction. The average speed of the robot is about 5 mm/s when a sawtooth signal with 5 kV amplitude and 2 Hz frequency is applied to the DE actuator.

Shengbin Wang

Department of Mechanical Engineering, University of Houston, 4800 Calhoun Rd, Houston, TX 77004

E-mail: swang62@uh.edu

*Zheng Chen, Corresponding Author Department of Mechanical Engineering, University of Houston, 4800 Calhoun Rd, Houston, TX 77004 E-mail: zchen43@central.uh.edu **Keywords** Biomimetics · Dielectric Elastomer Actuators · Flexible Robotics · Marine Robotics

1 Introduction

Recently, the ecological system in the ocean is rapidly changing due to global warming, pollution, over-fishing and the destruction of marine structures [1]. Biomimetic robots with high degrees of freedom, that can walk and swim smoothly in water, are greatly needed for underwater monitoring for applications such as pollution detection and video mapping [2]. Soft marine robots have some tremendous advantages in exploring and monitoring delicate marine ecosystems, like coral reefs without causing unintentional damage to fragile objects. Based on the envisioned underwater working conditions, jellyfish can be categorized to be one of the best choices for its energy efficiency, axisymmetric morphology, etc [3]. Jellyfish propulsive performance is related to the shape of its bell which can produce a combination of the vortex, rowing, and suction-based locomotion [4–7]. Jellyfish is capable of multiple types of locomotion with rhythmic motions of its umbrella bell, including moving upward and downward, which enables itself to adapt to various environmental conditions. Developing such jellyfish-like robot will help us better understand and monitor the oceanic environment and exploit marine resources.

The smart materials and advanced technology allow these interesting robots to achieve jellyfish-like morphology and movement. One of popular materials being utilized to develop the jellyfish robot is ionic polymer metal composite (IPMC) which can exhibit large dynamic deformation with the changing electric field [8]. Many researchers developed IPMCs which can provide actuation power and enlarged the movement of the bell for the jellyfish [9, 10]. Shi *et al.* developed a new jellyfish-like microrobot using eight IPMC

2 Shengbin Wang, Zheng Chen*

actuators as legs to resolve the problem of asymmetry in previous crawling microrobots [2]. However, the slow response time of IPMC causes a low contraction frequency on the bell, thus the maximum speed of IPMC-enabled jellyfish is limited. The jellyfish-like robot with flexible fins can also be equipped with permanent magnet for electromagnetic actuation [11] which induces a volumetric change of the deformable silicone cavity to expel a jet of fluid and produces positive thrust [12]. However, when the robot swims near some iron structures, the on-board permanent magnets will be attracted by these structures, which will disturb the motion of the robot. Takemura et al. [13] proposed another method to control the moving velocity of jellyfish by the chemical stimulation and controlled pulsation. Smart modular structure (SMS) combined with printed circuit boards (PCBs) and polyvinyl chloride polymer (PVC) had been used in a two layer jellyfish robot which can generate thrust by actuating the SMSs and recovery original state by relaxing and bending the SMSs [14]. To achieve a larger volume change, a new biomimetic underwater microrobot using shape memory actuator (SMA) was proposed in [15]. However, the mentioned robots consumes a large amount of power for heating, which is not energy efficient in underwater propulsion.

In contrast, the robotic jellyfish made by DE material combines many appealing features together, such as high compliance around 1 MPa [16], and fast response less than 200 μ s [17]. More than that, the recently developed selfsensing mechanism allows the robot to extract accurate displacement data during the actuation process with the information of capacitance [18, 19], the resistance of the circuit [20, 21], and current through the circuit [22]. The jellyfish robot made by DE actuator (DEA) has an excellent capability of electrical insulation between the actuators and drive electronics from the surrounding water. Some fabrication methods of the jellyfish robot with DE material have been proposed. An untethered jellyfish inspired soft robot was developed with an axisymmetric array of unimorph actuator [23]. One challenge of this jellyfish is to keep the eight lappets stable during the movement. Hareesh et al. [24] developed a DE jellyfish robot with chamber structure, simplified integrated design for robotic jellyfish fabrication was proposed by Tingyu et al. [25]. However, these previous studies are lack of theoretical models to analyze the experiment performance. . Utilizing the transmission mechanism to transform the movement from the DE actuators to the contraction of the bell is critical to improve the performance of the robot. With this proposed methodology, the swimming behavior of the jellyfish robot can be improved by revising the transmission mechanism, rather than only focusing on DE actuators.

This paper introduces a novel DE enabled jellyfish robot in terms of bio-inspired design, fabrication, and semi-

physics-based and date-driven modeling approach. The robot combines a double-layer DE membrane with a transmission mechanism to drive the bell to pump out the water and push it move upward. Furthermore, it can carry payload to swim, such as pressure sensor with mounting. The actuation mechanism of the jellyfish robot and the structure's deformation are very similar to one type of the true jellyfish (aurelia aurita). The buoyancy force can be provided by changing the volume of water that is under the jellyfish when a periodic sawtooth voltage is applied on the DE membranes. Benefiting from the geometry structure of the transmission, both of the DE membranes and jellyfish fins can produce propulsion for the jellyfish robot. Taking advantage of the good conductivity of water, the water in swimming pool is chosen as the negative electrode of the DE actuator and the positive electrode is isolated from the water and sealed inside of DE membrane. This paper also demonstrates a simplified modeling approach to capture the major multi-physics models involved in the robot, including the spring force model of cross-beam, volume change model of DE and bell structure, and water jet model. In the modeling work, each movement cycle is divided into two stages: bell relaxing step and bell contracting stage. A data-driven model using tfest function in MATLAB is developed to fit the experimental results in the first step. The second stage is analyzed by a physical model which can capture the volume changes within the bell when contracting. In both stages, the models can successfully predict experimental data. In order to analyze the speed performance under different frequencies, position measurements under sawtooth waveform with the same amplitude but different frequencies are conducted. Considering the limitation of the DE behavior in high frequency environment, the maximum speed of the robot under 2 Hz input voltage with sawtooth waveform can reach up to 5 mm/sec.

The structure of this paper is organized as following: Section 2 introduces the design and fabrication of the jellyfish robot. Section 3 provides modeling of the DE membrane and the actuation mechanism of the jellyfish. Section 4 demonstrates preliminary experimental results including frequency response, thrust force, and swimming speed characterization, two models are used to fit the experiment data. Section 5 discusses the conclusion of the paper and the future research for this jellyfish robot.

2 Design and Fabrication

The jellyfish robot fabricated in this paper mainly includes three parts: actuation system, moving structure, and transmission mechanism. The assembly of the jellyfish robot is shown in Fig. 1. The DE membrane, which is fabricated using a 3M VHB 4910 tape with compliant electrodes (carbon powder), provides actuation power. After the first pre-

stretching, the DE membrane's circumference is sealed between two plastic DE holders. The top middle part is secured by the cross flexible beam which is made of Acrylonitrile Butadiene Styrene (ABS) using 3D printer. The beam provides a support for the second pre-stretching of the DE membrane in vertical direction. The holes on the cross beam's surface can reduce fluid resistance. One side of a cylinder tube is attached to the middle of the DE membrane, and the other side is connected to eight supporting beams. Then the movement of the DE membrane is transferred to a soft umbrella fin by a transmission mechanism consisting of cylinder tube, hinged connections, and eight support beams. The contraction of the bell can provide upward propulsion for the robot. The fin is made of Thermoplastic Polyurethane (TPU) with a thickness of 0.4 mm, including eight segments that are pasted together by the VHB-F9473PC. It shows certain plastic deformation when it swings underwater. All links are hinged, and small hats are used to block the hinge connections to avoid looseness. The height of the jellyfish robot is approximately 170 mm and the maximize width of the robot is 240 mm.

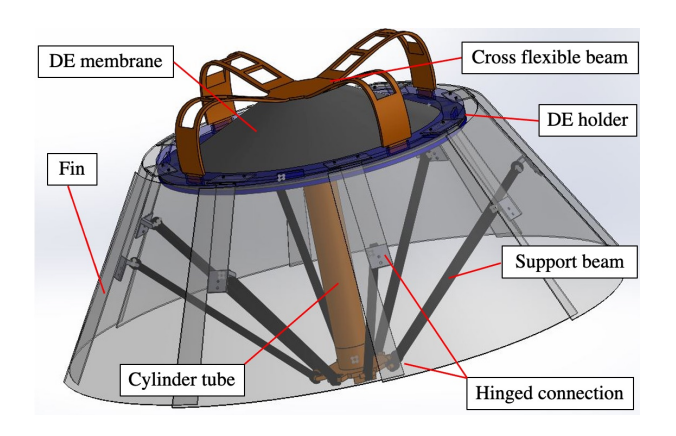


Fig. 1: Assembly of the jellyfish robot.

When a sawtooth voltage wave is applied on the DE membrane, the electrical field cross the DE membrane is transduced to a Maxwell stress which causes the DE membrane to decrease in thickness and increase in area. The spring-like cross flexible beam pulls the DE membrane along with the cylinder tube and support beams to move upward, resulting the expansion of the umbrella fin and inhalation of water. When the voltage disappears, the DE membrane returns to its original state, which pushes water out to produce thrust force. At the same time, the jellyfish fin contracts to exhale most of the water, which provides the propulsion to propel the jellyfish to move upward. The schematic of the procedure is shown in Fig. 2.

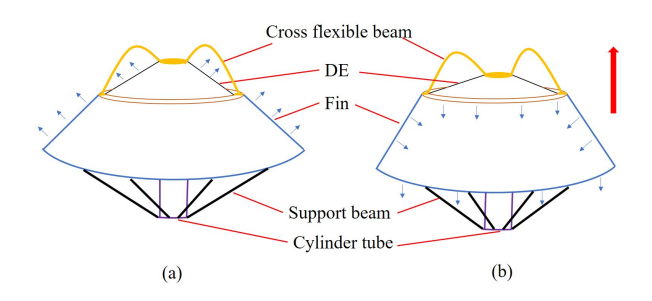


Fig. 2: The schematic of moving jellyfish: (a) voltage on (b) voltage off.

3 Modeling of the Jellyfish Robot

3.1 Cross-beam simplified model

The vertical pre-stretching of the DE membrane is supported by the flexible cross beam which is a 'negative-rate bias spring' or NBS. With a nonlinear bias force, this NBS system can decrease in stroke of less than 5% when the input rate increases from 1 to 10 Hz, indicating the NBS is a promising bias element when using in high-performance DE actuator [26]. Since the structure of the cross beam is irregular, it is difficult to directly calculate the force that the cross beam can provide when it changes its shape. Understandably, simplifying the cross beam to a common elastic object that can store mechanical energy is necessary. The cross beam is simplified into a linear spring in this paper. Once we assembled the cross flexible beam with the circle plastic support, we compressed the cross flexible beam from the top point O shown in Fig. 3. The maximize displacement we can get is h without destroying its structure, and the force we can get is F. Then according to Hooke's law F = kh, the spring constant k is obtained.

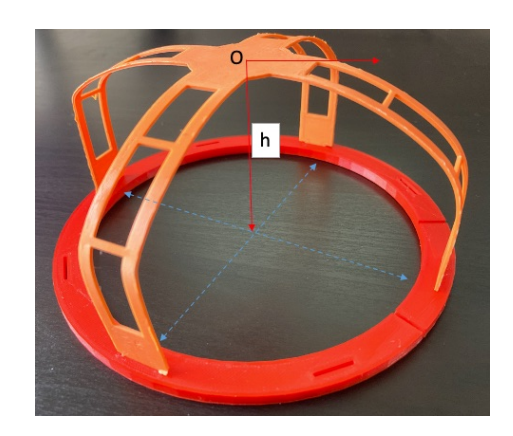


Fig. 3: Cross beam with circle plastic support.

3.2 DE membrane actuation model

The theoretical analysis based on the fabricated jellyfish robot provides simulation results and explains how the DE moves with its actuation when the electric power is applied on the jellyfish robot. The DE actuator has two layers of membrane as shown in Fig. 4, where one positive wire is sealed inside of the membranes and the negative electrode directly contacts with the water in the pool. The middle rigid frame is used to secure the two DE membranes to avoid separating or sliding from each other.

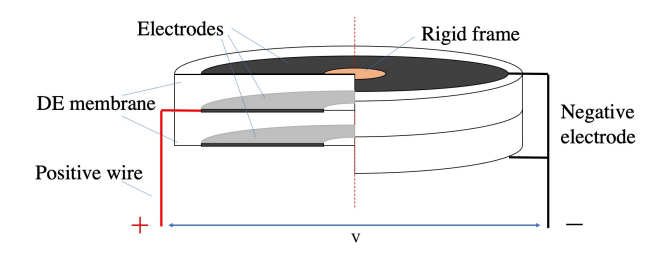


Fig. 4: DE membrane structure.

The two layers of DE membrane can double the output force comparing to one layer DE actuator. The overall actuator force can be determined based on force model of one circular. Fig. 5 shows the sectional view of the one layer actuator. The picture on the upper side shows the original state without voltage and vertical pre-stretching. The origin of coordinate axis system is built in the center of the circular frame to show the movement of the middle plate. A and B are the edges of the inner and outer of the circle support respectively. The radius of the middle plate is a, and the radius of the outside DE membrane is b. The description process of the simplified frustum DE actuator shown in Fig. 6.

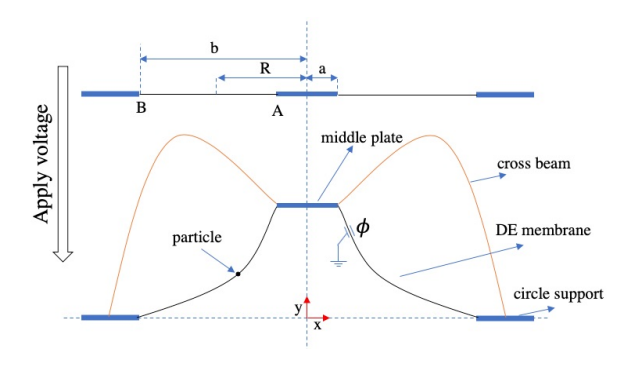


Fig. 5: Sectional view of one layer DE membrane.

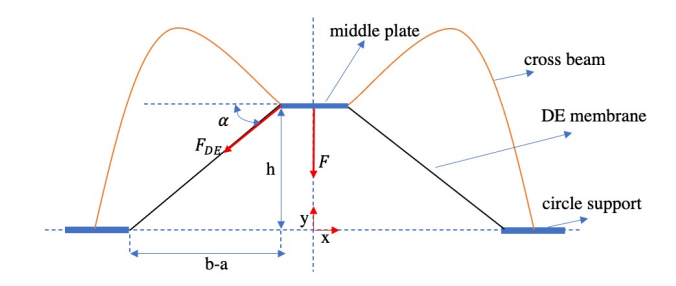


Fig. 6: Simplified DE membrane structure.

Assuming that the stress of the DE membrane in radial direction is σ_r , the force of one layer DE membrane is

$$F_{DE} = A\sigma_r = 2\pi r z \sigma_r,\tag{1}$$

where A is the cross-sectional area of DE membrane around the middle plate, z is the current thickness of the DE membrane, the total force of the two-layer DE membranes is $F=2F_{DE}$, and the force in the vertical direction is

$$F = 2F_{DE}\sin\alpha = 4\pi rz\sigma_r \frac{h}{\sqrt{h^2 + (b-a)^2}},$$
 (2)

where α is the angle between the DE membrane and horizontal direction.

The spring force from the cross beam and the total radius force from the DE membrane are changing dynamically when the voltage changes during the actuation process. The final dynamic equation comes from the vertical force equilibrium in the air, which can be computed as suggested from [27]

$$\ddot{h} = \frac{1}{m} [\bar{k}(H - h) - 4\pi rz \frac{h}{\sqrt{h^2 + (b - a)^2}} \sigma_r - mg - c\dot{h}], (3)$$

where H is the initial height of the cross beam, m is the total mass of the system, h is the displacement of the center plate, c is the damping constant of the system.

The dielectric elastomer membrane is assumed to be incompressible, λ_1 , λ_2 , λ_3 are used to represent the longitudinal stretches, circumferential stretches, and thickness stretches respectively. Let $\lambda_{1,pre}$, $\lambda_{2,pre}$, $\lambda_{3,pre}$ represent stretch of the first pre-stretching process, and $\lambda_{1,act}$, $\lambda_{2,act}$, $\lambda_{3,act}$ represent the vertical stretch considering the second pre-stretching and the actuation process, $\lambda_{1,tot}$, $\lambda_{2,tot}$, $\lambda_{3,tot}$ represent the total stretch. The relationships between each of the stretches can be calculated from Plante's paper [28]

$$\lambda_{1,tot} = \lambda_{1,pre}\lambda_{1,act},$$

$$\lambda_{2,tot} = \lambda_{2,pre}\lambda_{2,act},$$

$$\lambda_{3,tot} = \lambda_{3,pre}\lambda_{3,act},$$

$$\lambda_{1,tot}\lambda_{2,tot}\lambda_{3,tot} = \lambda_{1,pre}\lambda_{2,pre}\lambda_{3,pre}$$

$$= \lambda_{1,act}\lambda_{2,act}\lambda_{3,act} = 1.$$
(4)

The volume of the DE membrane is $V=\pi r_0^2 z_0$, r_0 is the original radius of the VHB tape before pre-stretching, and z_0 is the original thickness. Once the membrane is projected on the ground, the projection shape completely overlaps with the shape after the first pre-stretching. Therefore, it is reasonable to assume $\lambda_{2,act}=1$ and won't change all the time during the actuation process. After first circular prestretching, the stretch in different stages can be obtained as following

$$\lambda_{1,pre} = \frac{r_p}{r_0},$$

$$\lambda_{2,pre} = \frac{2\pi r_p}{2\pi r_0} = \frac{r_p}{r_0} = \lambda_{1,pre},$$

$$\lambda_{3,pre} = \frac{z_p}{z_0}.$$
(5)

where r_p and z_p are the radius and thickness of the tape respectively after the pre-stretching. In the second process, the values of three stretches can be calculated as

$$\lambda_{1,act} = \frac{l}{b-a} = \frac{\sqrt{(b-a)^2 + h^2}}{b-a},$$

$$\lambda_{2,act} = 1,$$

$$\lambda_{3,act} = \frac{z}{z_p}.$$
(6)

Combining (4), (5), (6), the new formulas to calculate the total stretches are defined as

$$\lambda_{1,tot} = \lambda_{1,pre} \lambda_{1,act} = \frac{r_p}{r_0} \frac{\sqrt{(b-a)^2 + h^2}}{b-a},$$

$$\lambda_{2,tot} = \lambda_{2,pre} \lambda_{2,act} = \frac{r_p}{r_0},$$

$$\lambda_{3,tot} = \lambda_{3,pre} \lambda_{3,act} = \frac{z}{z_p} \frac{z_p}{z_0} = \frac{z}{z_0}.$$
(7)

Following [29], the true stress σ_r in radius direction can be obtained as

$$\sigma_r = u(\lambda_{1,tot}^2 - \lambda_{1,tot}^{-2} \lambda_{2,tot}^{-2}) - \epsilon E^2,$$
 (8)

where the electric field E is

$$E = \frac{V}{z} = \frac{V}{z_p \lambda_{3,act}} = \frac{V \lambda_{1,act}}{z_p}.$$
 (9)

The direction of the water exhaled from the jellyfish is defined as negative direction, shown in Fig. 6. With (3), (6), (7), (8), (9), the acceleration of the middle plate can be obtained when the height of the cross beam and input voltage applied on the DE membrane such parameters are given.

$$\ddot{h} = \frac{1}{m} \{ \bar{k}(H - h) - 4\pi r \left(\frac{b - a}{\sqrt{(b - a)^2 + h^2}} \frac{r_0^2}{r_p^2} z_0 \right),$$

$$\frac{h}{\sqrt{h^2 + (b - a)^2}} u \left[\left(\frac{r_p}{r_0} \frac{\sqrt{(b - a)^2 + h^2}}{b - a} \right)^2,$$

$$- \left(\frac{r_p}{r_0} \frac{\sqrt{(b - a)^2 + h^2}}{b - a} \right)^{-2} \left(\frac{r_p}{r_0} \right)^{-2} \right],$$

$$- \epsilon \left(\frac{V \lambda_{1,act}}{z_p} \right)^2 - mg - c\dot{h} \}.$$
(10)

The original shape of the 4910 VHB tape is a diaphragm with a radius of $r_0 = 25$ mm. After the first circular prestretching, the radius becomes $r_p = 63$ mm. The original height of the cross beam is H = 60 mm, and rigid middle plate with radius a = 15 mm.

3.3 Water ejection model

The fin contracts and relaxes through the transmission mechanism powered by the movement of the DE membrane. Assuming that the fin is an ideal elastomer with a bell shape, the volume of the umbrella fin can be treated as a conical frustum. The radius of the top surface remains the same, while the bottom radius and the height of the conical frustum change when the umbrella fin moves. Fig. 7 shows the 2D section view of the simplified conical frustum where the solid line is the original state of the jellyfish and the dashed line is the final state. The volume of the water ejected from the conical frustum is mainly related to the angle change of the umbrella fin.

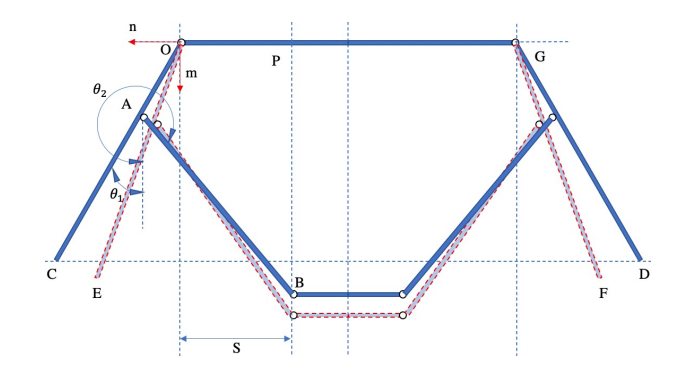


Fig. 7: Simplified umbrella fin with conical frustum.

The structure from the transmission part to the fin is equal to the offset slider-crank mechanism which can be used for velocity and acceleration analysis for the umbrella fin effectively. In Fig. 7, θ_1 is the angle between the OA and the positive direction of the m axis, θ_2 is the angle between AB and the positive direction of the m axis, and S is the offset length. The movement of point B is limited in the m direction, which is equal to the slider. OA can rotate around the point O, and OAB is similar to the crank. The estimated parameters of the simplified fin are shown in the Table 1.

3.3.1 Displacement analysis

From the closed vector polygon OABP, the vector equation is $\overrightarrow{OA} + \overrightarrow{AB} = \overrightarrow{OP} + \overrightarrow{PB}$, which can be transferred as complex function below

$$l_{OA}e^{i\theta_1} + l_{AB}e^{i\theta_2} = De^{i0} + Se^{i\pi/2}, \tag{11}$$

Table 1: Parameters of the conical frustum structure

Parameters	Value	Unit
θ_1	33.5	(Degree)
θ_2	318.5	(Degree)
l_{OA}	30	(mm)
l_{AB}	100	(mm)

where D is the distance between point B and the upside OG. Assuming the angular velocity of the fin is constant during each period of swinging, the angular acceleration is considered to be 0. Differentiating (11) about time t, the velocity of point B is given by

$$l_{QA}\omega_1 e^{i(\theta_1 + \pi/2)} + l_{AB}\omega_2 e^{i(\theta_2 + \pi/2)} = \dot{D},$$
 (12)

where ω_1 is the average angular velocity of the fin during each period and ω_2 is the angular velocity of AB around point A. From , the imaginary part of the equation (12) can be written as

$$l_{OA}\omega_1\cos\theta_1 + l_{AB}\omega_2\cos\theta_2 = 0, (13)$$

and the real part can be written as

$$-l_{OA}\omega_1\sin\theta_1 - l_{AB}\omega_2\sin\theta_2 = \dot{D}.$$
 (14)

Based on (13), the angular velocity of the AB can be represented by a function of ω_1

$$\omega_2 = \frac{-l_{OA}\omega_1\cos\theta_1}{l_{AB}\cos\theta_2}. (15)$$

Differentiating (14) with respect to time t, the acceleration function of point B can be derived by

$$\ddot{D} = l_{OA}\omega_1^2 e^{i(\theta_1 + \pi)} + l_{AB}\omega_2^2 e^{i(\theta_2 + \pi)} + l_{AB}\alpha_2 e^{i(\theta_2 + \pi/2)},$$
(16)

where α_2 is the angular acceleration of AB. The imaginary part of this function can be written as

$$-l_{OA}\omega_1^2 \sin \theta_1 - l_{AB}\omega_2^2 \sin \theta_2 + l_{AB}\alpha_2 \cos \theta_2 = 0, \quad (17)$$

the real part can be written as

$$-l_{OA}\omega_1^2 \cos \theta_1 - l_{AB}\omega_2^2 \cos \theta_2 - l_{AB}\alpha_2 \sin \theta_2 = a_B.$$
 (18)

The angular acceleration of the AB can be derived from (17)

$$\alpha_2 = \frac{l_{OA}\omega_1^2 \sin \theta_1}{l_{AB} \cos \theta_2} + \omega_2^2 \tan \theta_2. \tag{19}$$

Replacing α_2 in (18), the acceleration of point B can be calculated as below

$$a_B = -l_{OA}\omega_1^2 \cos \theta_1 - l_{AB}\omega_2^2 \cos \theta_2,$$

$$-l_{AB}(\frac{l_{OA}\omega_1^2 \sin \theta_1}{l_{AB} \cos \theta_2} + \omega_2^2 \tan \theta_2) \sin \theta_2.$$
 (20)

Comparing (3) and (20), \ddot{h} is equivalent to a_B . Both of them are the acceleration of point B on vertical direction. By combining the two groups of the function and replacing ω_2 with (15), ω_1 can be solved. The volume of water ejected from the jellyfish fin can be calculated by changing the volume of conical frustum from V_{OCDG} to V_{OEFG} , Where V_{OCDG} is the volume of conical frustum OCDG, and V_{OEFG} is the volume of conical frustum OEFG. They can be calculated following the same definition

$$V_{OCDG} = \frac{\pi h_1}{3} \left(\left(\frac{l_{OG}}{2} \right)^2 + \left(\frac{l_{CD}}{2} \right)^2 + \left(\frac{l_{OG}}{2} \right) \left(\frac{l_{CD}}{2} \right) \right), \quad (21)$$

$$h_1 = l_{OC} \cos(\theta_1),$$

where h_1 is the height of the conical frustum OCDG.

$$V_{OEFG} = \frac{\pi h_2}{3} \left(\left(\frac{l_{OG}}{2} \right)^2 + \left(\frac{l_{EF}}{2} \right)^2 + \left(\frac{l_{OG}}{2} \right) \left(\frac{l_{EF}}{2} \right) \right),$$

$$h_2 = l_{OE} \cos(\theta_1'),$$
(22)

where h_2 is the height of the conical frustum OEFG, and $\theta_1' = \theta_1 - \omega_1 T$ is the angle between the OE and m axis. For each period T, the average angle velocity is ω_1 , the volume change of the conical frustum over time is showing below

$$V_{eject1} = V_{OCDG} - V_{OEFG}. (23)$$

The final volume of the water eject from the umbrella fin V_{eject1} can be calculated by combining (20), (21), (22), (23).

$$V_{eject1} = \frac{\pi l_{OC} \cos(\theta_1)}{3} \left\{ \left(\frac{l_{OG}}{2}\right)^2 + \left(\frac{l_{OG}}{2} + l_{OC} \sin \theta_1\right)^2, + \left(\frac{l_{OG}}{2}\right) \left(\frac{l_{OG}}{2} + l_{OC} \sin \theta_1\right) \right\} - \frac{\pi l_{OE} \cos(\theta_1 - \omega_1 T)}{3},$$

$$\left\{ \left(\frac{l_{OG}}{2}\right)^2 + \left[\frac{l_{OG}}{2} + l_{OE} \sin(\theta_1 - \omega_1 T)\right]^2, + \left(\frac{l_{OG}}{2}\right) \left[\frac{l_{OG}}{2} + l_{OE} \sin(\theta_1 - \omega_1 T)\right] \right\}.$$
(24)

The shape of simplified DE membrane is also similar to a conical frustum, as shown in Fig. 8. The volume of water

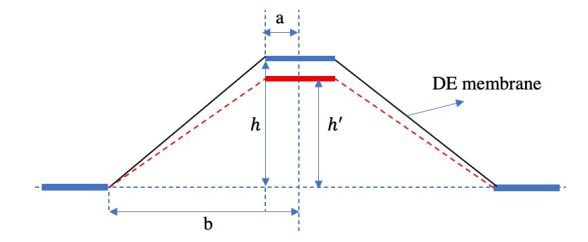


Fig. 8: Shape change of the DE membrane.

ejected from the DE membrane can be calculated as

$$V_{eject2} = \frac{\pi(h - h')}{3}(a^2 + b^2 + ab), \tag{25}$$

where h is the max height of the DE membrane, $h^{'}$ is the current DE membrane height when it returns back to its original state after the voltage is off. The total volume of the water eject from the jellyfish is

$$V_{eject} = V_{eject1} + V_{eject2}. (26)$$

The buoyancy force in the vertical direction can be calculated based on Archimedes principle

$$F_{buoyance} = \rho V_{eject} g. \tag{27}$$

where ρ is the density of the water, and g is the gravity.

4 Experimental Results

Several experiments have been implemented to testify the behavior of the jellyfish robot. Due to the natural behaviors of jellyfish — fast contraction and slow relaxation, a time-varying sawtooth wave is an ideal input signal to drive the jellyfish robot to generate the same dynamic movement as the real jellyfish. Comparing with general signals (sinusoidal or square), the sawtooth is most related to the bioinspired signal. The bell expands slowly in the slope of the sawtooth wave, and contracts suddenly in the vertical part. However, because of the elasticity property of the DE material, the DE membrane restores to its original shape slowly during the actuation process. If the frequency is too low, the time taken actuation to respond will be much less. Hence the deflection in each cycle will reduce with increasing frequency. In this paper, 2 Hz frequency is chosen for the driving signal, the amplitude of the voltage is limited to 5 kV. There are two phases in the jellyfish robot movement. One is the contraction phase in which the DE membrane is compressed when the voltage is slowly applied on the DE membrane in each period. Another phase is called propulsion phase in which the DE membrane recovers to its original shape after voltage is off. During this phase, the jellyfish robot ejects the water and generates thrust force to push the jellyfish to move upward.

4.1 Frequency response of the DE membrane actuator

The actuation parts of the jellyfish robot include the DE membrane and the stiff circle plate as well as the cross beam showing in Fig. 9. The cross beam provides the vertical prestretching for the DE membrane, which have been simplified to be a spring-mass-damper system in the Section 3. To determine the characteristics of the DE membrane actuator,

a system identification to estimate the transfer function of the actuator is performed. This is achieved by analyzing the system's frequency response of the actuator over the range of 0.05 Hz to 16 Hz with sinusoidal input signal. The full voltage range (0-5000 V) input to the DE membrane actuator is normalized between 0 to 1. The frequency responses are the same when different amplitudes are applied [22]. 0.8 input magnitude is chosen in this paper. The response is then plotted on the bode magnitude plot and a transfer function is fitted onto the data. The actuation voltage is provided by a high voltage amplifier (HVA 10HVA24-BP1-F), the real displacement of the DE tube is measured by a laser sensor (Baumer OADM 20I6441/S14F), data acquisition is implemented in real-time by using Simulink and dSPACE (DS1104, dSPACE Inc.).

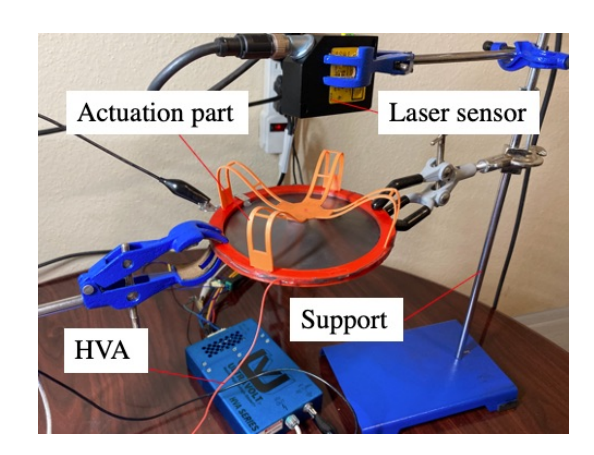


Fig. 9: Frequency response measurement setup.

The magnitude of the frequency response is obtained by using Fast Fourier Transform (FFT) method, Fig. 10 shows the bode plot of the measured frequency response results. A third-order transfer function with three poles and one zero

$$G(s) = \frac{77680s + 135300}{s^3 + 802.3s^2 + 73020s + 109500}$$
 (28)

is used to fit all of the experiment data by minimizing the mean square error from the experiment data points. Since the cut-off frequency of the transfer function is around 10 Hz, a 2 Hz actuation signal is within the actuation frequency range of the DE actuator.

4.2 Thrust force measurement

In this section, the thrust force generated by the robot is measured. The simulation results from combining models are compared with the experiment results. The experimental setup is shown in Fig. 11. The force created by the jellyfish in the vertical direction is computed by the load cell (ATI

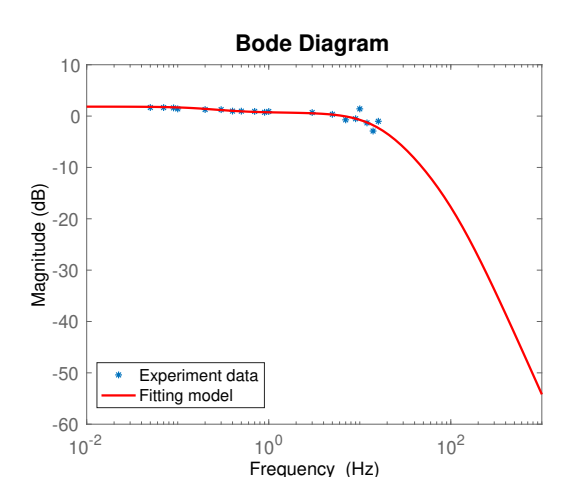


Fig. 10: Frequency response of the jellyfish actuation.

FT23747). The experiment results are collected by National Instruments DAQ. A stable weight is added to stabilize the plate that is attached to the force sensor. The remaining components are from the frequency response experiment.

Fig. 12 shows that the force is produced when 2 Hz and 5 kV sawtooth voltage applies on the DE membrane. The experimental data shows the thrust force at the steady state.

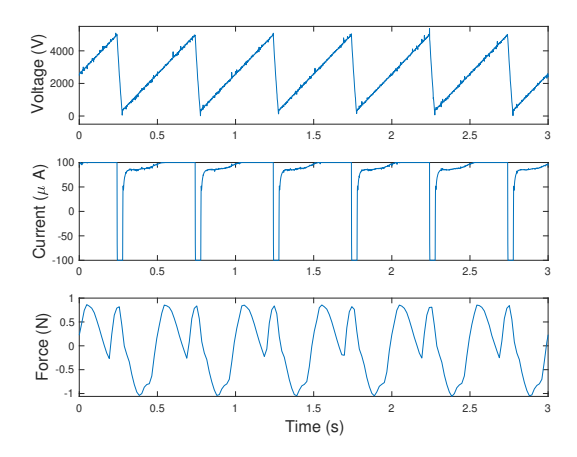


Fig. 12: The experiment results with sawtooth wave at 2 Hz and 5 kV.

In this paper, we did an experiment with 15 periods in total. The first ten periods were chose for training to get transfer function to capture the dynamic movement in the first step, the left five periods were chose for testing to evaluate the experimental data fitting formula. Fig. 13 indicates that the experiment data roughly overlap and have a certain trajectory in one cycle. Different colored points are used to distinguish each period. The positive thrust force means the

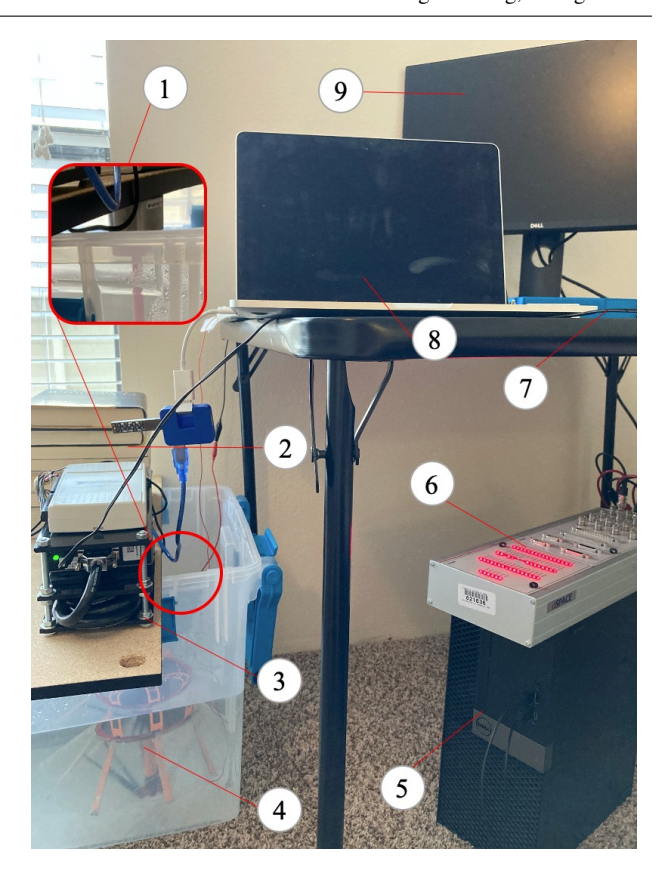


Fig. 11: Propulsive force measurement setup (1): Force sensor. (2): Stable weight. (3): Data acquisition. (4): Jellyfish robot. (5) Desktop(control input signal). (6): dSPACE. (7) HVA(High Voltage Amplify). (8) Force result display. (9) Electric result display.

direction of the force is downward, while the negative force means the direction of the force is upward. Based on the experiment results, the detail movement process can be divided into two steps shown in Fig. 14, where a vibration included in the first step, the blue rectangular bar S_0 presents the original state of jellyfish fin, the red rectangular bar S_1 presents the final state. The red arrow is the movement direction, the number with circle is the order of the movement in each step. Due to the influence of inertia, the force may experience vibration when inhaling water to decrease the buoyancy force, as we can see from Fig 14(a).

For the first step, a second order transfer function with time delays (29) is used to capture the dynamic movement of the jellyfish, which is recognized by tfest function in MATLAB.

$$Sys(s) = e^{(-0.304s)} \frac{0.9193}{s^3 + 4.384s^2 + 305.3}.$$
 (29)

The process of exhaling water to increase buoyancy force is approximately 0.15 second as shown in Fig. 14(b). The start point of its simulation follows the end point of

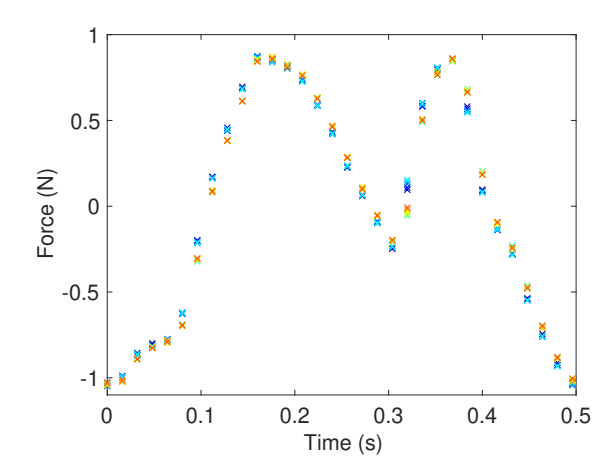


Fig. 13: Experiment data overlapping in one cycle.

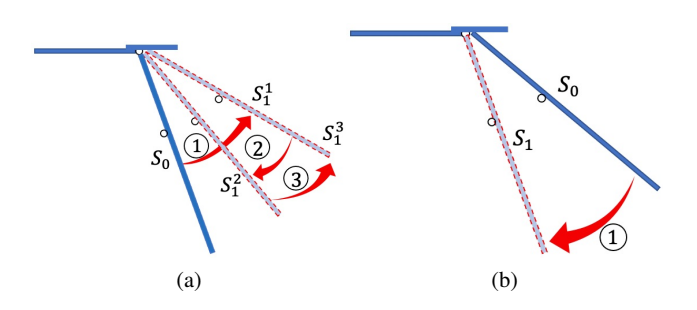


Fig. 14: Two steps of the movement.

the first step simulation result. The detailed physical models have been introduced in Section 3, parts of the simulation parameters are listed in Table 2. The final results with the remaining testing experiment data and all of the simulation results are shown in Fig. 15. The blue line is the simulation result from (29), the red line is the simulation result based on the physical models above. The simulation results fits the experiment data perfectly, and the maximum change of the buoyancy force is approximately 2 N.

Table 2: Parameters of jellyfish robot

Parameters	Value	Unit
Permittivity, ϵ	4×10^{-11}	(Fm^{-1})
Shear modulus, u	27450	(Nm^{-2})
Damping coefficient, c	10	(Ns/m)
Mass, m	100	(g)
l_{OG}	120	(mm)
l_{OC}	90	(mm)
Gravity, g	9.81	(m/s^2)
Density, ρ	997	(kg/m^3)

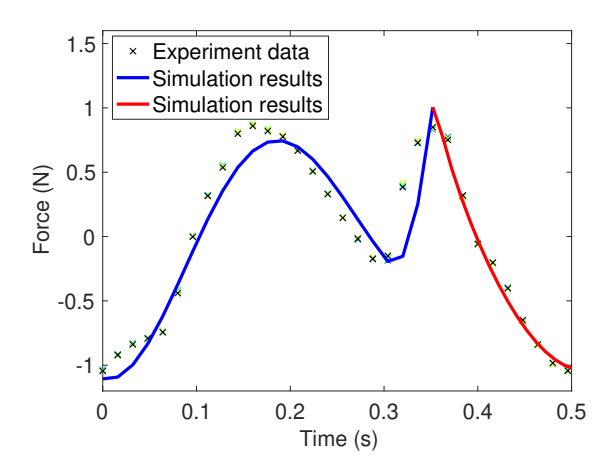


Fig. 15: Simulation results and experiment data.

4.3 Comparison with low frequency sawtooth signals

The frequency of the input signal also influences the movement effect of the jellyfish robot. A sawtooth wave with 1 Hz and 5 kV amplitude is applied on the jellyfish, the experimental results are shown in Fig. 16.

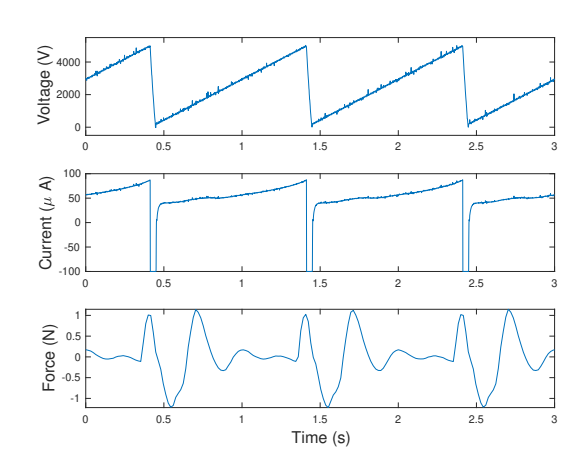


Fig. 16: Results with 5 kV sawtooth and 1 Hz wave.

The sampling frequency of the force sensor is 62.5 Hz, the displacement is zero under force-free motion. At the beginning of the experiment, the jellyfish robot is adjusted to be neutral buoyancy with no displacement at the best effort. Assuming that the force F_s produced by the jellyfish is constant, the force can be measured by the force sensor in each of the sampling period $T_s=1/62.5$ s. Therefore, the acceleration of the jellyfish in each period can be calculated as

$$a_i = \frac{F_s}{m},\tag{30}$$

where m is the mass of the jellyfish. Defining v_i as the initial velocity of the jellyfish for each cycle, then the velocity at the end of the cycle is $v_{i+1} = v_i + a_j T_s$. The increased displacement for the jellyfish during the period is

$$D_i = v_i T_s + \frac{1}{2} a_i T_s^2 = \frac{(v_i + v_{i+1})}{2} T_s.$$
 (31)

The work energy of the force produced in each period can be calculated as follows:

$$W_i = F_s D_i. (32)$$

The experiments demonstrate the movement of the jellyfish from the stationary state to the final stable periodic motion state, which is also maintained for a certain time of period. The final work energy combines both states' results - Combined Work Energy (CWE) is shown in table 3. As one can see from the table, only the sawtooth signal with sufficient high frequency can push the jellyfish to move upward when its CWE is negative. This also proves previous statements that the jellyfish can not move upward when the frequency is too low due to the elasticity property of the DE material.

Table 3: Work energy results.

Signal	Combine Work Energy(CWE)	Units
Sawtooth (1Hz)	0.001691565	(J)
Sawtooth (2Hz)	-0.003488088	(J)

4.4 Velocity with certain frequency and amplitude signals

The movement of the jellyfish robot is then measured by combining the pressure sensor and the electric input signal. The code for the experiments is stored in Arduino. The output results are collected by the CoolTerm software. The type of the pressure sensor is MS5803-14BA. The water surface atmospheric pressure P_0 can be measured at the beginning of the experiment before the pressure sensor is put inside of the water and stored in the Arduino. From the underwater pressure formula $P=\rho gh$, one can calculate the depth of the jellyfish robot as

$$h = \frac{(P - P_0)}{\rho g}. (33)$$

where P is the pressure of jellyfish robot's position in water, g is the gravity, and ρ is the density of the water. The values of g and ρ are the same with previous experiment. The experiment setup is shown in Fig. 17.

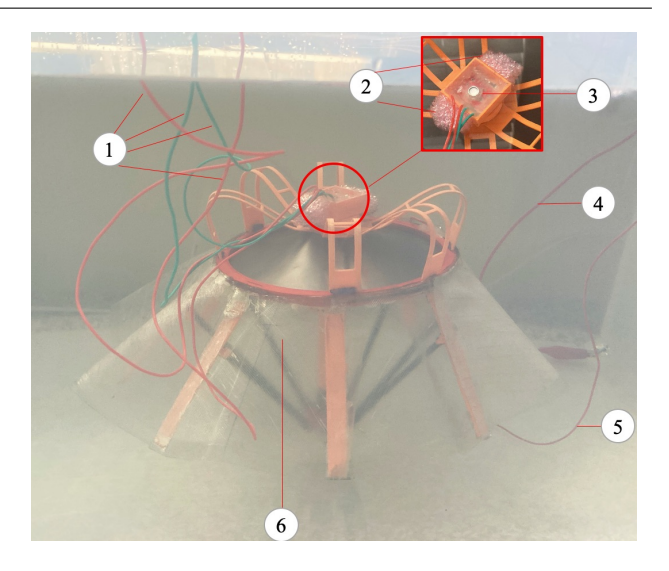


Fig. 17: Experiment setup for the speed test (1): Wires for pressure sensor. (2): Float for the robot. (3): Pressure sensor. (4): Negative wire connected with water. (5) Positive wire connect robot. (6): Jellyfish robot.

Four experiments with pressure sensor are conducted using the same amplitude input sawtooth signal and different frequency. The jellyfish robot reaches its highest point at different times. The experiment results are shown in Fig. 18.

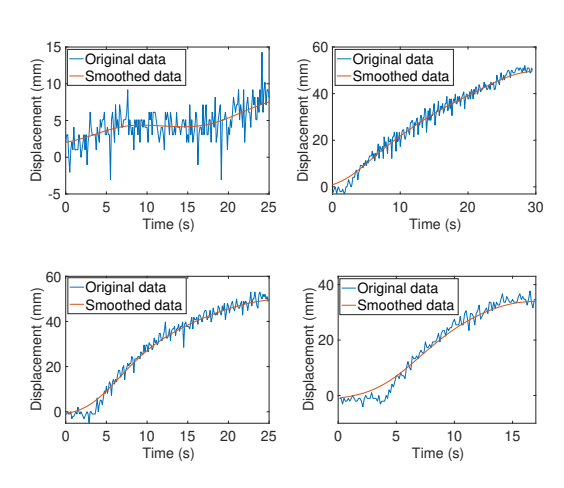


Fig. 18: Experimental results with 5 kV sawtooth and 1.4 Hz, 1.6 Hz, 1.8 Hz and 2.0 Hz, respectively.

From the experiment results, the average speeds of the jellyfish under different frequencies are determined to be: 0.024 mm/s under 1.4 Hz input signal, 1.6 mm/s under 1.6 Hz input signal, 2 mm/s under 1.8 Hz input signal, and 2.05 mm/s under 2 Hz input signal. The result shows that the speed of the jellyfish increases when frequency is higher. However, there are reduction of deflection in each cycle un-

der high frequency [12] and unsubstantial speed increase when approaching 2 Hz, the frequency is set to be 2 Hz.

Another experiment without pressure sensor is documented on camera, where the weight is less than the jellyfish with the pressure sensor and the actuation behaviour of the DE membrane is not affected by the sensor mounting. The sawtooth voltage wave with 5 kV amplitude and 2 Hz frequency is used to drive the jellyfish robot, the movement of robot shown in Fig. 19. In the first picture, the jellyfish robot is at negative buoyancy, and stays in the bottom of the water tank. After the voltage is applied on the membrane for two seconds, the jellyfish moves about 20 mm upward. After ten seconds, the jellyfish robot approaches to the surface of the water with a moving distance of 50 mm. The velocity of the jellyfish decreases when it approaching the surface of the water. One of the reason of being is that the water turbulence becomes intense when the jellyfish approaches to the surface. The average velocity of the jellyfish within the 10 second range is 5 mm/s which is faster than the jellyfish with a pressure sensor.

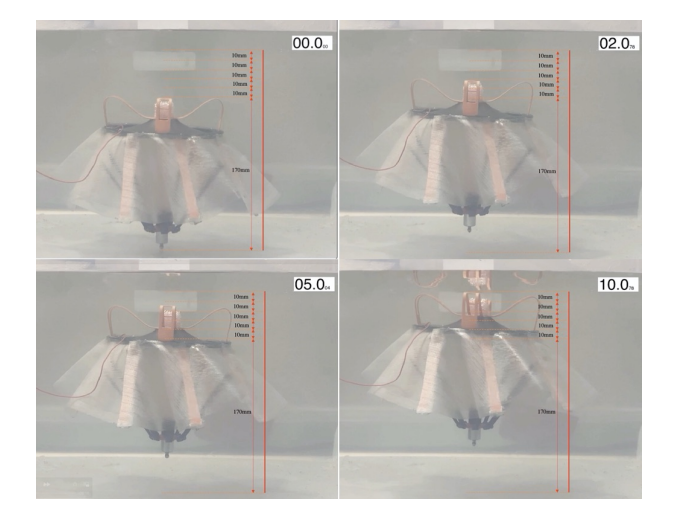


Fig. 19: Snapshots of jellyfish robot's movement.

5 Conclusion

A bio-inspired jellyfish robot based on dielectric elastomer material is developed in this research. With the help of the performance of DE material and the transmission structure, the jellyfish robot can mimic the swimming mechanism to inhale and eject water to push the robot to move upward and also carry payload to swim. The contraction and relaxation of the umbrella fin of the jellyfish robot can be accomplished by controlling the sawtooth voltage applied on the DE membrane. Meanwhile, water is ejected from the DE membrane to induce propulsion. A physical model, based on the simplified jellyfish structure, incorporated with a second order

transfer function is proposed to analyze the actuation mechanism of the robot in different steps. The preliminary experiment results have shown that the soft robot with multi-layer DE membranes can move effectively in water. The performance of the jellyfish is influenced by many factors, such as the frequency of the input signal, fabrication of the DE membrane, the pre-stretching, and the total weight of the jellyfish. In further research, the behavior of the jellyfish under high frequency signal will be explored. Developing a stabler model to capture different kinds of input signal, increasing the speed of the jellyfish, and controlling the movement direction as well as the speed of the jellyfish will also be studied in future work.

Acknowledgements This work was supported by the National Science Foundation under Grant CMMI #1747855.

References

- D. Kim, J.-U. Shin, H. Kim, D. Lee, S.-M. Lee, and H. Myung, "Development of jellyfish removal robot system jeros," in *Proc.* of 2012 9th International Conference on Ubiquitous Robots and Ambient Intelligence, 11 2012, pp. 599–600.
- L. Shi, S. Guo, and K. Asaka, "Development of a new jellyfishtype underwater microrobot." *I. J. Robotics and Automation*, vol. 26, 01 2011.
- 3. B. Gemmell, K. Du Clos, S. Colin, K. Sutherland, and J. Costello, "The most efficient metazoan swimmer creates a 'virtual wall' to enhance performance," *Proceedings of the Royal Society B: Biological Sciences*, vol. 288, p. 20202494, 01 2021.
- 4. J. Frame, N. Lopez, O. Curet, and E. Engeberg, "Thrust force characterization of free swimming soft robotic jellyfish," *Bioinspiration and Biomimetics*, vol. 13, p. 064001, 09 2018.
- B. Gemmell, D. Troolin, J. Costello, S. Colin, and R. Satterlie, "Control of vortex rings for manoeuvrability," *Journal of The Royal Society Interface*, vol. 12, 07 2015.
- S. Colin and J. Costello, "Morphology, swimming performance and propulsive mode of six co-occurring hydromedusae," *The Journal of experimental biology*, vol. 205, pp. 427–37, 03 2002.
- B. Gemmell, S. Colin, J. Costello, and J. Dabiri, "Suction-based propulsion as a basis for efficient animal swimming," *Nature Communications*, vol. 6, 11 2015.
- 8. M. Shahinpoor and K. Kim, "The effect of surface-electrode resistance on the performance of ionic polymer-metal composite (ipmc) artificial muscles," *Smart Materials and Structures*, vol. 9, p. 543, 08 2000.
- J. Najem, A. Sarles, B. Akle, and D. Leo, "Biomimetic jellyfishinspired underwater vehicle actuated by ionic polymer metal composite actuators," *Smart Materials Structures - SMART MATER* STRUCT, vol. 21, 09 2012.
- S.-W. Yeom and I.-K. Oh, "A biomimetic jellyfish robot based on ionic polymer metal composite actuators," Smart Materials and Structures, vol. 18, p. 085002, 06 2009.
- Y. Ko, S. Na, Y. Lee, K. Cha, S. Y. Ko, J.-O. Park, and S. Park, "A jellyfish like swimming mini robot actuated by an electromagnetic actuation system," *Smart Materials and Structures*, vol. 21, p. 057001, 04 2012.
- K. Marut, C. Stewart, T. Michael, A. Villanueva, and S. Priya, "A jellyfish inspired jet propulsion robot actuated by an iris mechanism," *Smart Materials and Structures*, vol. 22, p. 094021, 08 2013.

- R. Takemura, Y. Akiyama, T. Hoshino, and K. Morishima, "Chemical switching of jellyfish-shaped micro robot consisting only of cardiomyocyte gel," 2011 16th International Solid-State Sensors, Actuators and Microsystems Conference, TRANSDUCERS'11, pp. 2442–2445, 06 2011.
- 14. Y. Zhou, H. Jin, C. Liu, E. Dong, M. Xu, and J. Yang, "A novel biomimetic jellyfish robot based on a soft and smart modular structure (sms)," in *Proc. of 2016 IEEE International Conference* on Robotics and Biomimetics, 12 2016, pp. 708–713.
- L. Shi, S. Guo, and K. Asaka, "A novel butterfly-inspired underwater microrobot with pectoral fins," 2011 IEEE International Conference on Mechatronics and Automation, ICMA 2011, 08 2011.
- J. Shintake, H. Shea, and D. Floreano, "Biomimetic underwater robots based on dielectric elastomer actuators," in *Proc. of 2016* IEEE/RSJ International Conference on Intelligent Robots and Systems, 10 2016, pp. 4957–4962.
- L. Maffli, S. Rosset, M. Ghilardi, F. Carpi, and H. Shea, "Ultrafast all polymer electrically tunable silicone lenses," *Advanced Func*tional Materials, vol. 25, 03 2015.
- S. Wang, T. Kaaya, and Z. Chen, "Self-sensing of dielectric elastomer tubular actuator with feedback control validation," Smart Materials and Structures, 05 2020.
- G. Rizzello, D. Naso, A. York, and S. Seelecke, "Closed loop control of dielectric elastomer actuators based on self-sensing displacement feedback," *Smart Materials and Structures*, vol. 25, p. 035034, 02 2016.
- B. O'Brien, J. Thode, I. Anderson, E. Calius, E. Hämmerle, and S. Xie, "Integrated extension sensor based on resistance and voltage measurement for a dielectric elastomer," *Proceedings of SPIE*- *The International Society for Optical Engineering*, 04 2007.
- T. Hoffstadt and J. Maas, "Adaptive sliding mode impedance and position control for dielectric elastomer transducers," in *Proc. of* the SPIE Conference on Electroactive Polymer Actuators and Devices (EAPAD), 03 2018, p. 105940Y.
- Z. Ye and Z. Chen, "Self-sensing of dielectric elastomer actuator enhanced by artificial neural network," Smart Materials and Structures, vol. 26, 07 2017.
- C. Christianson, C. Bayag, G. Li, S. Jadhav, A. Giri, C. Agba, T. Li, and M. Tolley, "Jellyfish-inspired soft robot driven by fluid electrode dielectric organic robotic actuators," *Frontiers in Robotics and AI*, vol. 6, p. 126, 11 2019.
- G. Hareesh, J. Li, Y. Wang, and J. Zhu, "A soft jellyfish robot driven by a dielectric elastomer actuator," *IEEE Robotics and Automation Letters*, vol. 1, pp. 1–1, 07 2016.
- T. Cheng, G. Li, Y. Liang, M. Zhang, B. Liu, T. W. Wong, J. Forman, M. Chen, G. Wang, Y. Tao, and T. Li, "Untethered soft robotic jellyfish," *Smart Materials and Structures*, vol. 28, 11 2018.
- M. Hodgins, A. York, and S. Seelecke, "Experimental comparison of bias elements for out-of-plane deap actuator system," *Smart Materials and Structures*, vol. 22, p. 094016, 08 2013.
- M. Hodgins, G. Rizzello, D. Naso, A. York, and S. Seelecke, "An electro-mechanically coupled model for the dynamic behavior of a dielectric electro-active polymer actuator," *Smart Materials and Structures*, vol. 23, p. 104006, 09 2014.
- J.-S. Plante and S. Dubowsky, "Large-scale failure modes of dielectric elastomer actuators," *International Journal of Solids and Structures - INT J SOLIDS STRUCT*, vol. 43, 04 2006.
- T. He, L. Cui, C. Chen, and Z. Suo, "Large deformation analysis of a dielectric elastomer membrane-spring system," *Smart Materials and Structures*, vol. 19, p. 085017, 07 2010.